Reversal of orbital angular momentum arising from an extreme Doppler shift

Graham M. Gibson[a,1,2], Ermes Toninelli[a,1], Simon A. R. Horsley[b], Gabriel C. Spalding[c], Euan Hendry[b], David B. Phillips[a,b], and Miles J. Padgett[a]

[a]School of Physics and Astronomy, University of Glasgow, Glasgow G12 8QQ, United Kingdom; [b]Electromagnetic Materials Group, Department of Physics, College of Engineering, Mathematics and Physical Sciences, University of Exeter, Exeter, Devon EX4 4QL, United Kingdom; and [c]Department of Physics, Illinois Wesleyan University, Bloomington, IL 61701

Edited by David A. Weitz, Harvard University, Cambridge, MA, and approved February 27, 2018 (received for review November 28, 2017)

The linear Doppler shift is familiar as the rise and fall in pitch of a siren as it passes by. Less well known is the rotational Doppler shift, proportional to the rotation rate between source and receiver, multiplied by the angular momentum carried by the beam. In extreme cases the Doppler shift can be larger than the rest-frame frequency and for a red shift, the observed frequency then becomes "negative." In the linear case, this effect is associated with the time reversal of the received signal, but it can be observed only with supersonic relative motion between the source and receiver. However, the rotational case is different; if the radius of rotation is smaller than the wavelength, then the velocities required to observe negative frequencies are subsonic. Using an acoustic source at ≈100 Hz we create a rotational Doppler shift larger than the laboratory-frame frequency. We observe that once the red-shifted wave passes into the "negative frequency" regime, the angular momentum associated with the sound is reversed in sign compared with that of the laboratory frame. These low-velocity laboratory realizations of extreme Doppler shifts have relevance to superoscillatory fields and offer unique opportunities to probe interactions with rotating bodies and aspects of pseudorelativistic frame translation.

Doppler | acoustic | orbital angular momentum | negative frequency | time reversal

In 1981 Garetz considered the rotational analogue to the well-known Doppler effect (1). Normally discussed in terms of circularly polarized light, this rotational frequency shift is a geometrical effect equivalent to the observation that if placed into a rotating frame, the second hand of a watch appears to revolve at a different frequency. For an electromagnetic wave, this rotational effect arises from the angular momentum of the wave which can be either intrinsic (spin) or extrinsic (orbital) (2–4). In experiments using millimeter-wave sources, an angular velocity of Ω between the rest frame of the source and the observer gave rise to an angular frequency shift of $\Delta\omega = (\sigma + \ell)\Omega$, where $\sigma\hbar$ and $\ell\hbar$ are, respectively, the spin angular momentum (where $\sigma = \pm 1$) and the orbital angular momentum (OAM) of the photons (5). Here ℓ is an unbounded integer characterizing the azimuthally dependent phase of the field $e^{i\ell\theta}$, where θ is the azimuthal coordinate, resulting in such a beam possessing ℓ-fold rotational symmetry. This rotational Doppler effect has also been observed in light carrying OAM backscattered from a rotating rough surface, enabling the remote measurement of an object's rate of rotation (6–8).

Waves possessing OAM are not restricted to optical fields and, for example, have been observed acoustically (9, 10). As with the well-known linear case, the rotational Doppler shift can also be observed both optically and acoustically (11, 12). In the acoustic case, the longitudinal nature of the wave means that the angular momentum can be only orbital and hence the frequency shift is simply $\Delta\omega = \ell\Omega$, where ℓ/ω_0 is the ratio between the angular momentum and energy of the wave, and ω_0 is the frequency of the sound field in the rest frame of the source (13).

In the present work we investigate the unusual situation in which the rotational Doppler shift becomes larger than the rest-frame frequency of the source itself. We create an acoustic wave carrying OAM (14, 15) and then observe its Doppler-shifted frequency ω_D in a rotating frame: $\omega_D = \omega_0 + \ell\Omega$ (16). When ℓ and Ω are of opposite sign and $|\ell\Omega| > \omega_0$, the magnitude of the frequency shift is larger than the rest-frame frequency and consequently ω_D becomes negative. However, experimentally we measure $|\omega_D|$. Therefore, as the Doppler-shifted frequency ω_D becomes increasingly negative, the measured frequency $|\omega_D|$ becomes increasingly positive. However, despite $|\omega_D|$ being unsigned, the negative frequency still has a physical interpretation: When ω_D becomes negative, the OAM observed in the rotating frame undergoes a reversal in handedness (i.e., sign). Furthermore, at yet higher Doppler shifts when $|\ell\Omega| > 2\omega_0$, we observe that the measured acoustic Doppler-shifted frequency $|\omega_D|$ becomes blue shifted with respect to ω_0, regardless of the handedness of the OAM or the sense of rotation. Similar sign reversals have been discussed in the linear case, where a supersonic velocity between a source and an observer results in a temporal reversal of the transmitted signal (17–19). By contrast, we find that in the rotational case, supersonic motion is not

Significance

The emergence of "negative" frequencies in physical systems is often accompanied by intriguing consequences. For example, supersonic motion between a source and an observer leads to a negative Doppler-shifted frequency, the physical meaning of which is time reversal of the received signal. To our knowledge, the rotational analogue of this situation—the consequences of generating negative rotationally Doppler-shifted waves—has not been studied. Here we show, using an acoustic source, that a negative rotational Doppler shift is associated with a handedness reversal of the orbital angular momentum carried by the wave. We demonstrate that this handedness reversal can occur even at significantly subsonic velocities, making our findings relevant to interactions of ultrafast rotating systems with optical frequency radiation.

Author contributions: G.M.G., E.T., E.H., and M.J.P. designed research; G.M.G., E.T., G.C.S., E.H., and D.B.P. performed research; E.T., S.A.R.H., and D.B.P. analyzed data; G.M.G., E.T., D.B.P., and M.J.P. wrote the paper; S.A.R.H. modeled acoustic fields; and E.T. realized the 16-channel sound generation and stereo Bluetooth sound capture.

The authors declare no conflict of interest.

This article is a PNAS Direct Submission.

Data deposition: The data reported in this paper have been deposited at dx.doi.org/10.5525/gla.researchdata.577.

[1]G.M.G. and E.T. contributed equally to this work.

[2]To whom correspondence should be addressed. Email: graham.gibson@glasgow.ac.uk.

This article contains supporting information online at www.pnas.org/lookup/suppl/doi:10.1073/pnas.1720776115/-/DCSupplemental.

required when the transverse motion of the microphone takes place in a superoscillatory region of the acoustic field, i.e., where the lateral distance between phasefronts is less than the acoustic wavelength (20).

Results

Fig. 1 shows a schematic of our experimental setup. A ring of 16 loudspeakers, each of which can be independently phase shifted, was used to create a sound wave carrying OAM at the output of the acoustic waveguides. To probe the sound field in a rotating frame, two microphones were mounted on a rotatable disk and placed in the acoustic field. The two microphones were positioned with a common radius but having a small angular displacement $\delta\theta_{mic} \sim 0.2$ rad. This enabled both the OAM magnitude and handedness of the rotationally Doppler-shifted frequencies to be measured.

As an example, a phase delay of $\pi/2$ rad between each of the 16 adjacent speakers creates an acoustic beam carrying OAM corresponding to $\ell = -4$. As we are using a discretized array to shape the acoustic field, we also generate lower-power sidebands centered around the target OAM value, separated in OAM index by n, the number of sources (hence the nearest sidebands are located at $\ell = -20$ and $\ell = +12$ in our case) (21). The rotational Doppler effect can then be observed by tracking peaks in the Fourier spectra of the temporal signals recorded by the rotating microphones. These Doppler-shifted frequencies reveal the OAM spectrum of the acoustic field in the rotating frame (22). Fig. 2*A* shows a sonogram displaying these Fourier spectra for a range of microphone rotation rates. Fig. 2*B* shows examples of the Fourier spectrum of the microphones' temporal responses at particular angular velocities. In Fig. 2*A* the brightness of the traces represents the modulus of each component of the first microphone's Fourier spectrum, and the color of the trace encodes the phase difference between the signals recorded by the two microphones. *Explanation of All Peaks Found in Fourier Transforms of Microphone Signals* gives further explanation of all of the peaks present in Fig. 2.

Initially the rotatable disk is static, and we observe only a single peak in the Fourier spectra at the fundamental acoustic frequency ω_0. Upon rotating the microphones, we observe this fundamental acoustic frequency separates into a number of different peaks, indicating that the measured signal is now formed from a range of different frequency components. Each of these components corresponds to a rotational Doppler shift associated with a specific value of OAM present in the structured acoustic field. As we have directed the majority of the power into the $\ell = -4$ mode, this is the brightest component visible in Fig. 2*A*. We rotate the microphones in the same sense as the OAM carried by the $\ell = -4$ mode and therefore initially observe the $\ell = -4$ mode undergo a red shift (i.e., to a lower frequency). In addition to the sidebands due to the discretization of the source array, we also observe other peaks in Fig. 2*A*, centered around $\ell = 0$. These peaks correspond to rotational Doppler shifts of additional lower-power components in the OAM decomposition of the field. These additional components arise due to residual misalignments between the axis of rotation of the microphones and the axis of the speaker ring, as well as any other imperfections in the speaker arrangement.

As the two microphones are rotated the Fourier transforms of their measured signals exhibit frequency-dependent phase differences $\delta\phi$. These phase differences are due to the signal recorded by the second microphone lagging behind that recorded by the first one. Given that the microphones are closely spaced, these phase differences are proportional to the OAM value: $\delta\phi = \ell \cdot \delta\theta_{mic}$. Therefore, plotting the phase differences between the two microphones as a function of frequency reveals the OAM of the field associated with each modal component, as shown in the color key in Fig. 2*A*.

At a microphone rotation rate of $\Omega = 141$ rad/s ($F = 22.5$ Hz), the measured frequency of the $\ell = -4$ component falls to zero, since at this rotation rate, the rotational Doppler shift is exactly equal in magnitude to the fundamental acoustic frequency $\omega_0 = 565$ rad/s ($f_0 = 90$ Hz). As the angular velocity of the microphones is further increased, $\Omega > 141$ rad/s, this modal component now rises in frequency, but the mode itself is observed to have a reversed OAM and has switched from $\ell = -4 \rightarrow \ell = +4$.

Finally, when $\Omega > 282$ rad/s ($F > 45$ Hz), we observe that the $\ell = -4 \rightarrow \ell = +4$ component is blue shifted with respect to the laboratory-frame acoustic frequency ω_0. At this combination of rotation rate and OAM, a blue shift occurs irrespective of the handedness of the OAM or the sense of rotation of the microphone.

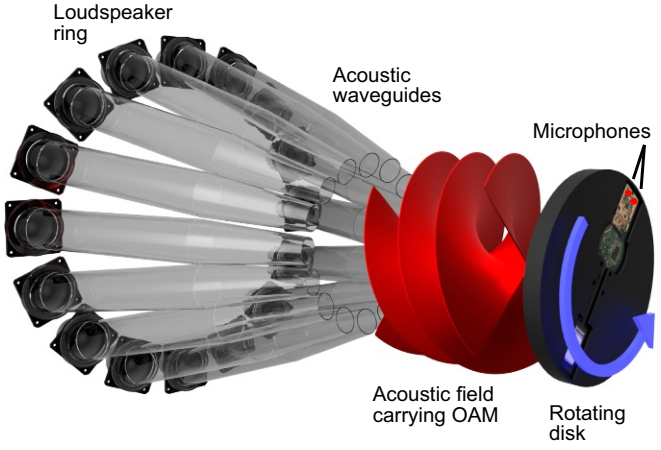

Fig. 1. Experimental setup. A ring of 16 loudspeakers (ring diameter $D_{spk} \sim 0.47$ m) is used to create acoustic fields carrying OAM. A set of tapered acoustic waveguides channels the sound to a smaller-diameter ring (diameter $D_{mic} \sim 0.19$ m) where the acoustic field is probed by two microphones mounted in a rotating disk. An audio Bluetooth module allows signals to be acquired from the microphones as the disk is rotated [rotation rate is increased in increments of 0.25 Hz up to 55 Hz ($\Omega = 345$ rad/s)].

Discussion and Conclusions

There are some intriguing contrasts between the emergence of Doppler inversion phenomena in the linear case and that in the rotational case. The linear Doppler-shifted frequency f_D is given by

$$f_D = \frac{c + v_r}{c + v_s} f_0, \qquad [1]$$

where c is the speed of sound in the propagation medium, f_0 is the rest-frame acoustic frequency, and v_r and v_s are the velocities of the receiver and source, respectively. In Eq. **1**, f_D becomes negative only when the relative speed between the source and the observer is supersonic. When such a negative frequency occurs with the linear Doppler effect, its physical meaning is a time reversal of the received signal. This phenomenon famously led Lord Rayleigh to observe that if a source moves toward a static listener at a rate of $v_s = 2c$, a piece of music being transmitted by that source would be heard reversed in time by the listener, while still retaining the correct tempo and pitch (17).

In contrast to the linear Doppler shift, the onset of a negative frequency in the rotational Doppler shift does not exhibit a time reversal. This is because there is no relative motion along the axis between the source and the receiver, and so no mechanism exists by which the propagating waves can be time reversed. Instead, as discussed above and shown in Fig. 2, in the rotational case such a negative frequency is associated with an azimuthal mode

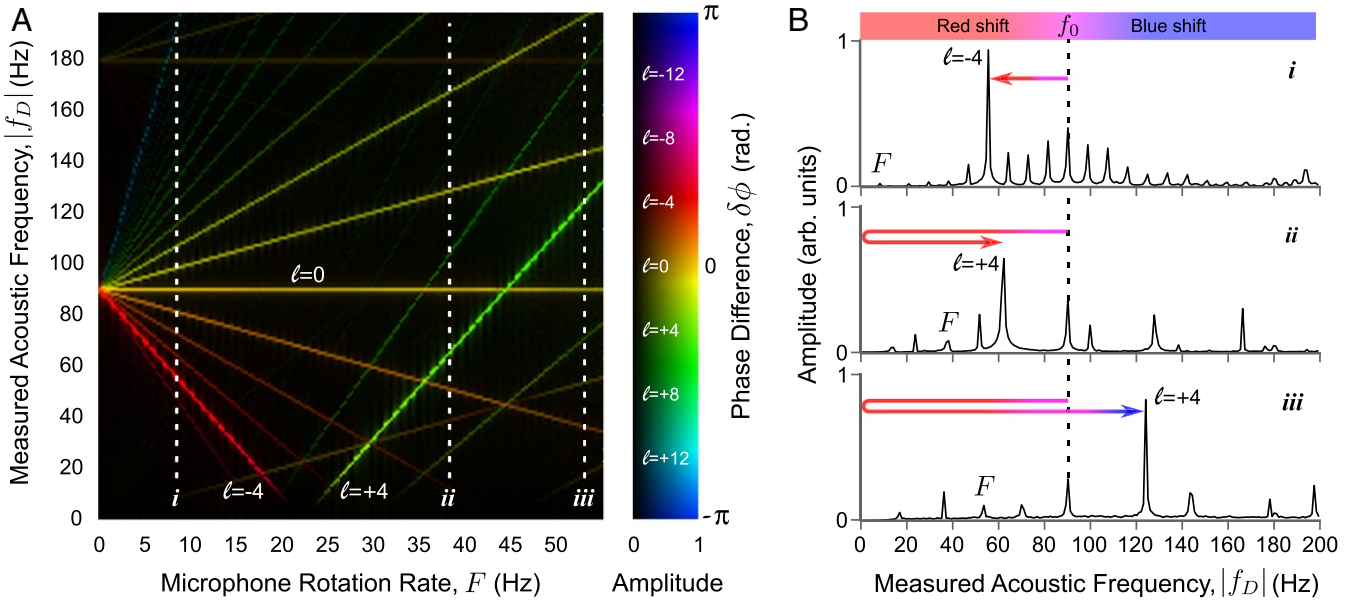

Fig. 2. Experimental observation of OAM handedness reversal in a rotating frame. (*A*) Sonogram showing the Fourier spectra of the recorded temporal signals for different rotation rates, *F*, of the microphones, where $F = \Omega/2\pi$. Here the measured acoustic frequency $|f_D| = |\omega_D|/2\pi$. The brightness of the features represents the modulus of the spectral components of the signal recorded by the first microphone, and the color represents the phase difference, $\delta\phi$, between the signals from both microphones. At low frequencies we observe a reduction in amplitude (brightness) due to a roll-off in the microphones' frequency response. (*B*) The amplitude of individual Fourier spectra from the key points *i–iii* indicated on the sonogram. In this experiment the fundamental acoustic frequency was ω_0 = 565 rad/s (i.e., $f_0 = \omega_0/2\pi = 90$ Hz).

inversion: The handedness (i.e., sign) of the OAM is reversed. This handedness reversal can occur even with a subsonic transverse microphone velocity (v_t): The radius of the trajectory followed by the microphones in our experiment was r = 95 mm. This means we are probing a superoscillatory region of the field (i.e., a region where the transverse phase gradient is greater than that of a plane wave) (20). This can be understood by considering that there is a critical radius of the circular orbit, r_c, above which the microphones' transverse velocity is supersonic:

$$r_c = \frac{c}{\Omega}. \qquad [2]$$

The rotation rate at which we observe the OAM inversion in our experiment is 22.5 Hz (Ω = 141 rad/s). At this rotation rate, the radius of the circle above which the microphones' transverse velocity would be supersonic is r = 2.4 m. However, in our experiment, the transverse velocity (v_t) of the microphones positioned at r = 95 mm is far below the speed of sound: $v_t \sim 0.04c$.

As described above, to achieve $\omega_D < 0$, we require that ℓ and Ω are of opposite sign and $|\ell\Omega| > \omega_0$. Therefore, substituting for Ω in Eq. **2** yields

$$r_c = \frac{|\ell|\lambda}{2\pi}. \qquad [3]$$

Eq. **3** describes the radius of a circle with a circumference equal to $|\ell|\lambda$. We can see that the magnitude of r_c is of the same order and shares the same scaling with λ, as the diffraction limit d of a tightly focused acoustic beam ($d \sim \lambda/2$). This comparison of radii highlights how the relative rotation rate between the source and receiver is intimately linked to the diffraction limit when considering OAM reversal phenomena in the rotational Doppler effect.

The unusual effects observed here in the acoustic regime are a rather general feature of wave physics and have implications for the interaction of light with ultrafast rotating systems. In particular, Eq. **3** shows that an OAM handedness reversal may potentially be observable at optical frequencies for subwavelength-scale objects rotating with nonrelativistic transverse velocities. For example, Korech et al. (23) measured the rotational Doppler shift due to rotating nitrogen and deuterium molecules, finding a Doppler shift in the terahertz range, six orders of magnitude greater than previously measured in mechanically rotating birefringent crystals (24, 25). In the future, similar experiments with lower-frequency sources or hotter molecular gases could potentially access the regime where an extreme Doppler shift results in the apparent OAM handedness changing sign. We therefore anticipate that the effects that we predict may soon need to be taken into account at optical frequencies.

Furthermore, Doppler inversion also has implications for rotation detection: refs. 6 and 8 showed that waves carrying OAM reflected from a spinning body encode information about the body's rotation rate. By measuring the rotational Doppler shift of these reflected waves, the rotation rate of the object can be measured via the relation $\omega_D = \omega_0 + \ell\Omega$. Our work highlights that the measurement of the Doppler shift, ω_D, of a wave carrying a single value of OAM (ℓ) gives rise to an ambiguity in the detected rotation rate; i.e., even if the rotation direction is known, we cannot distinguish between $\Omega_1 = \ell^{-1}(\omega_D - \omega_0)$ and $\Omega_2 = -\ell^{-1}(\omega_D + \omega_0)$. To lift this degeneracy, we must measure the Doppler shift imparted to waves carrying at least two different values of OAM.

Finally we note that negative frequencies due to large Doppler shifts have been considered in several other systems, including in hydrodynamic (26, 27) and optical (28) regimes. The interest in the emergence of negative-frequency waves in these contexts is related to predictions in quantum field theory and the amplification of incident waves, creating a link with Hawking radiation (27) or Penrose superradiance (29, 30) and the Zel'dovich effect (31, 32) in the case of rotation. In this work we have shown that negative frequencies are readily accessible acoustically, which may provide opportunities to investigate these exotic effects.

In summary, we have demonstrated that a negative rotationally Doppler-shifted frequency gives rise to a reversal in the

handedness of the angular momentum carried by the wave. This is the rotational analogue to the time reversal observed upon the onset of negative frequency in the linear case. We emphasize that this is a nonrelativistic effect, which, in contrast to the linear case, can occur even when the associated transverse velocities are well below the velocity of the wave. This effect could lead to an ambiguity in the detected rotation rate of a spinning object and in the future may be of relevance to the interpretation of rotational molecular spectra and the frequency spectra from opto-mechanical systems undergoing ultrafast rotation.

The raw data for this article can be found in an open-access repository at dx.doi.org/10.5525/gla.researchdata.577.

ACKNOWLEDGMENTS. We thank University of Glasgow physics technicians Paul Agnew and John Marshall for help with initial rotation experiments using a metalworking lathe. We also thank Ewan Wright and Daniele Faccio for useful discussions with respect to the Zel'dovich effect. This work was supported by the European Research Council (TWISTS, Grant 192382). D.B.P. acknowledges support from the Royal Academy of Engineering. E.T. acknowledges support from the Engineering and Physical Sciences Research Council (EPSRC) Center for Doctoral Training in Intelligent Sensing and Measurement (EP/L016753/1).

1. Garetz BA (1981) Angular Doppler effect. *J Opt Soc Am* 71:609–611.
2. Beth RA (1936) Mechanical detection and measurement of the angular momentum of light. *Phys Rev* 50:115–125.
3. Friese MEJ, Nieminen TA, Heckenberg NR, Rubinsztein-Dunlop H (1998) Optical alignment and spinning of laser-trapped microscopic particles. *Nature* 394:348–350.
4. Allen L, Beijersbergen MW, Spreeuw RJC, Woerdman JP (1992) Orbital angular momentum of light and the transformation of Laguerre-Gaussian laser modes. *Phys Rev A* 45:8185–8189.
5. Courtial J, Robertson DA, Dholakia K, Allen L, Padgett MJ (1998) Rotational frequency shift of a light beam. *Phys Rev Lett* 81:4828–4830.
6. Lavery MPJ, Speirits FC, Barnett SM, Padgett MJ (2013) Detection of a spinning object using light's orbital angular momentum. *Science* 341:537–540.
7. Rosales-Guzmán C, Hermosa N, Belmonte A, Torres JP (2013) Experimental detection of transverse particle movement with structured light. *Sci Rep* 3:2815.
8. Phillips DB, et al. (2014) Rotational Doppler velocimetry to probe the angular velocity of spinning microparticles. *Phys Rev A* 90:011801.
9. Nye JF, Berry MV (1974) Dislocations in wave trains. *Proc R Soc A* 336:165–190.
10. Volke-Sepúlveda K, Santillán AO, Boullosa RR (2008) Transfer of angular momentum to matter from acoustical vortices in free space. *Phys Rev Lett* 100:024302.
11. Courtial J, Dholakia K, Robertson DA, Allen L, Padgett MJ (1998) Measurement of the rotational frequency shift imparted to a rotating light beam possessing orbital angular momentum. *Phys Rev Lett* 80:3217–3219.
12. Skeldon KD, Wilson C, Edgar M, Padgett MJ (2008) An acoustic spanner and its associated rotational Doppler shift. *New J Phys* 10:013018.
13. Demore CEM, et al. (2012) Mechanical evidence of the orbital angular momentum to energy ratio of vortex beams. *Phys Rev Lett* 108:194301.
14. Anhäuser A, Wunenburger R, Brasselet E (2012) Acoustic rotational manipulation using orbital angular momentum transfer. *Phys Rev Lett* 109:034301.
15. Marzo A, et al. (2015) Holographic acoustic elements for manipulation of levitated objects. *Nat Commun* 6:8661.
16. Speirits FC, Lavery MPJ, Padgett MJ, Barnett SM (2014) Optical angular momentum in a rotating frame. *Opt Lett* 39:2944–2946.
17. Strutt Baron Rayleigh JW (1896) *The Theory of Sound* (Macmillan, London), Vol 2.
18. Nemiroff RJ (2015) Superluminal spot pair events in astronomical settings: Sweeping beams. *Publ Astron Soc Aust* 32:e001.
19. Clerici M, et al. (2016) Observation of image pair creation and annihilation from superluminal scattering sources. *Sci Adv* 2:e1501691.
20. Dennis MR, Hamilton AC, Courtial J (2008) Superoscillation in speckle patterns. *Opt Lett* 33:2976–2978.
21. Liu R, et al. (2015) Discrete emitters as a source of orbital angular momentum. *J Opt* 17:045608.
22. Zhou H-L, et al. (2017) Orbital angular momentum complex spectrum analyzer for vortex light based on the rotational Doppler effect. *Light Sci Appl* 6:e16251.
23. Korech O, Steinitz U, Gordon RJ, Averbukh IS, Prior Y (2013) Observing molecular spinning via the rotational Doppler effect. *Nat Photon* 7:711–714.
24. Arita Y, Mazilu M, Dholakia K (2013) Laser-induced rotation and cooling of a trapped microgyroscope in vacuum. *Nat Commun* 4:3374.
25. Mazilu M, et al. (2016) Orbital-angular-momentum transfer to optically levitated microparticles in vacuum. *Phys Rev A* 94:053821.
26. Rousseaux G, et al. (2010) Horizon effects with surface waves on moving water. *New J Phys* 12:095018.
27. Weinfurtner S, Tedford EW, Penrice MCJ, Unruh WG, Lawrence GA (2011) Measurement of stimulated Hawking emission in an analogue system. *Phys Rev Lett* 106:021302.
28. Rubino E, et al. (2012) Negative frequency resonant radiation. *Phys Rev Lett* 108:253901.
29. Penrose R (1969) Gravitational collapse: The role of general relativity. *Rivista del Nuovo Cimento, Numero Speziale I* 257; reprinted (2002) *General Relativity and Gravitation* 34:1141–1165.
30. Torres T, et al. (2017) Rotational superradiant scattering in a vortex flow. *Nat Phys* 13:833–836.
31. Zel'dovich Y (1971) Generation of waves by a rotating body. *ZhETF Pisma Redaktsiiu* 14:270–272.
32. Faccio D, Wright EM (2017) Nonlinear Zel'dovich effect: Parametric amplification from medium rotation. *Phys Rev Lett* 118:093901.